iScience

CellPress
OPEN ACCESS

Article

Self-propelled predator-prey of swarming Janus micromotors

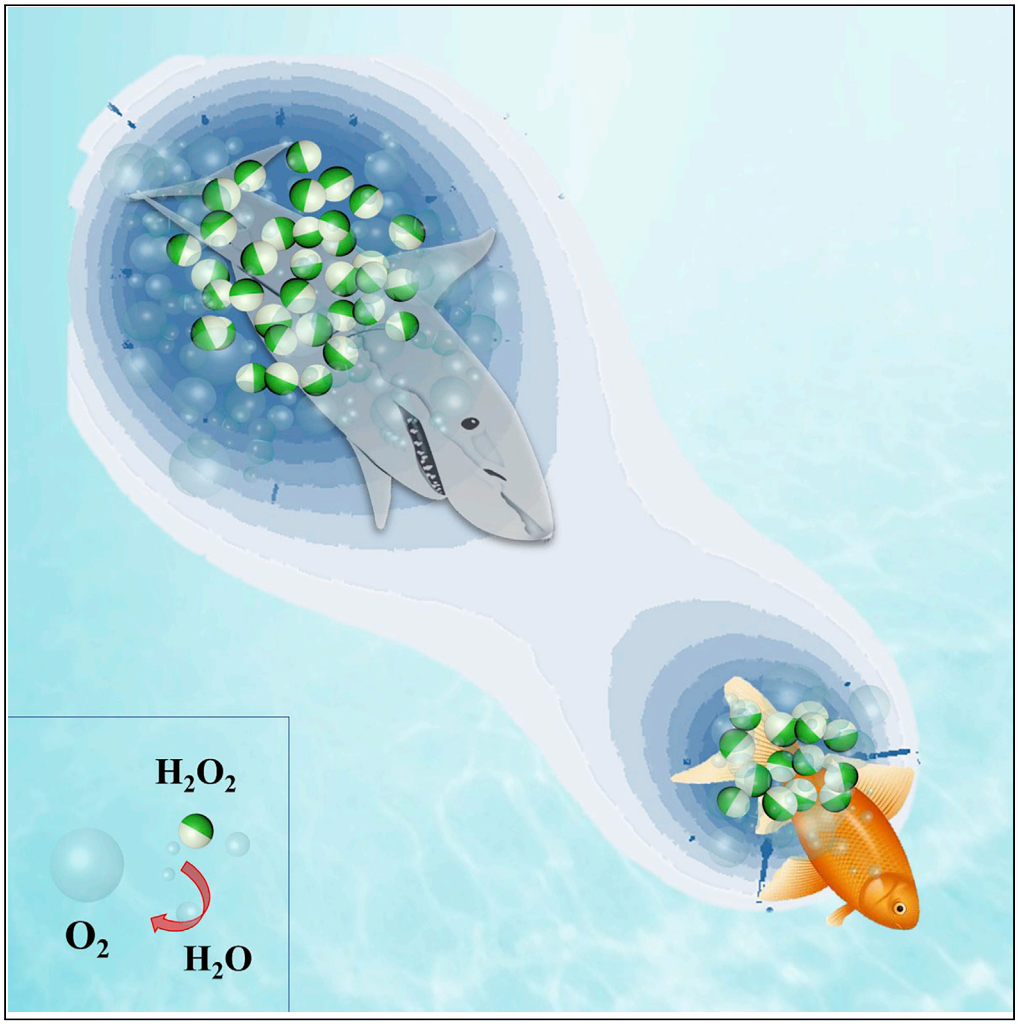

Tieyan Si, Zhenwei Wu, Wenping He, Qiang He

tieyansi@hit.edu.cn (T.S.)
6020170122@jsnu.edu.cn (W.H.)

Highlights

We synthesized self-propelled clusters of swarming Janus micromotors

A self-propelled cluster of swarming Janus micromotors predates another cluster

The cluster confined to the substrate surface moves much faster than that in bulk solution

Si et al., iScience *26*, 106112
March 17, 2023
https://doi.org/10.1016/j.isci.2023.106112

iScience

CellPress
OPEN ACCESS

Article

Self-propelled predator-prey of swarming Janus micromotors

Tieyan Si,[2,4,5,*] Zhenwei Wu,[2] Wenping He,[1,*] and Qiang He[2,3]

SUMMARY

It is a long-standing challenge to accomplish bionic microrobot that acts in a similar way of white blood cell, chasing bacteria in complex environment. Without an effective external control field, most swarming microrobots systems are usually unable to perform directional movement and redirect their motion to capture the target. Here we report the predatory-prey dynamics of self-propelled clusters of Janus micromotors. The active cluster generates an oxygen bubbles cloud around itself by decomposing H_2O_2, which levitated it above the substrate, enhancing its mobility in solution to wander around to devour other clusters. The fast decomposition of H_2O_2 also induced a tubular low-concentration zone that bridges two clusters far separated from each other, resulting in a diffusio-osmotic pressure that drives the two clusters to meet. This predatory-prey phenomena mimic white blood cells chasing bacteria and swarming flocks in nature, shedding light on emergent collective intelligence in biology.

INTRODUCTION

Collective motions of many self-propelled individuals in nature including bird flocks,[1] fish swarms, honey bee schools,[2,3] swarming bacteria, and active microswimmers[4–7] demonstrate emergent collective intelligence. Swarming microswimmers based on different propulsion mechanisms perform complex self-propelled motions and self-assembled ordered phases in response to environmental stimuli. Self-organizing schools of many individual fishes change their collective morphology to forage or escape from danger according to environmental changes.[8] The mechanism by which complex collective intelligence emerges out of many simple individuals is one of the most intricate mysteries in science owing to many uncontrollable biological factors. However, artificial micromotors/nanomotors provide a promising way to mimic biological collective intelligence in the laboratory and reveal its underlying mechanisms.[9–11]

Collective swarming of micromotors/nanomotors can be triggered by external stimuli such as magnetic fields,[12–14] light,[9,15,16] ultrasound,[17–19] electric fields,[20,21] and chemicals,[22–25] thus providing diverse manipulation methods for biosensors, cargo transportation, drug delivery,[11,26,27] and many collectively ordered processes. For example, peanut-shaped hematite motors self-organize into ribbons when triggered by blue light[16] and transform into vortex and strip patterns under alternating magnetic fields.[14] These collective patterns are also found in the swarming colloidal motors of rod-shaped eutectic gallium-indium alloy (EGaIn) liquid metal in a modulating acoustic field,[18] which form a round liquid-like microswarm that transforms reversibly between different configurations.[14,28] Communication between individual micromotors/nanomotors plays a key role in forming a collective pattern. An ion-exchange reaction is an effective method of communication in swarms of nanorods and nanoparticles[19] and induces the interaction between ZnO nanorods and sulfonated poly styrenesulfonate (PS) microbeads.[29] Phototaxis is a common phenomenon in nature. Guan and co-workers reported artificial phototactic Janus TiO_2/Si microswimmers operating independently that were capable of biomimicry. They found that the passive silica particles actively sought out and swam toward AgCl particles in a manner similar to predator-prey behavior between two species of passive microparticles in the absence of chemical fuels and external fields.[11,30–32] Even though Ultraviolet (UV) light can stimulate reversible aggregation and dispersion of swarming Janus micromotors,[15,33] it is still a major challenge to realize active predator-prey phenomena in a micromotor system without global external stimuli.

Here we report predator-prey dynamics between clusters of swarming Janus micromotors in hydrogen peroxide (H_2O_2). The Janus micromotor is a polyelectrolyte multilayer-modified SiO_2 microsphere that is

[1]The Key Laboratory of Biotechnology for Medicinal Plants of Jiangsu Province and School of Life Science, Jiangsu Normal University, Xuzhou, Jiangsu 221116, PR China

[2]Key Laboratory of Micro-Systems and Micro-Structures Manufacturing, Ministry of Education, Harbin Institute of Technology, Harbin 150080, China

[3]School of Medicine and Health, Harbin Institute of Technology, Harbin 150080, China

[4]School of Physics, Harbin Institute of Technology, Harbin 150080, China

[5]Lead contact

*Correspondence: tieyansi@hit.edu.cn (T.S.), 6020170122@jsnu.edu.cn (W.H.)

https://doi.org/10.1016/j.isci.2023.106112

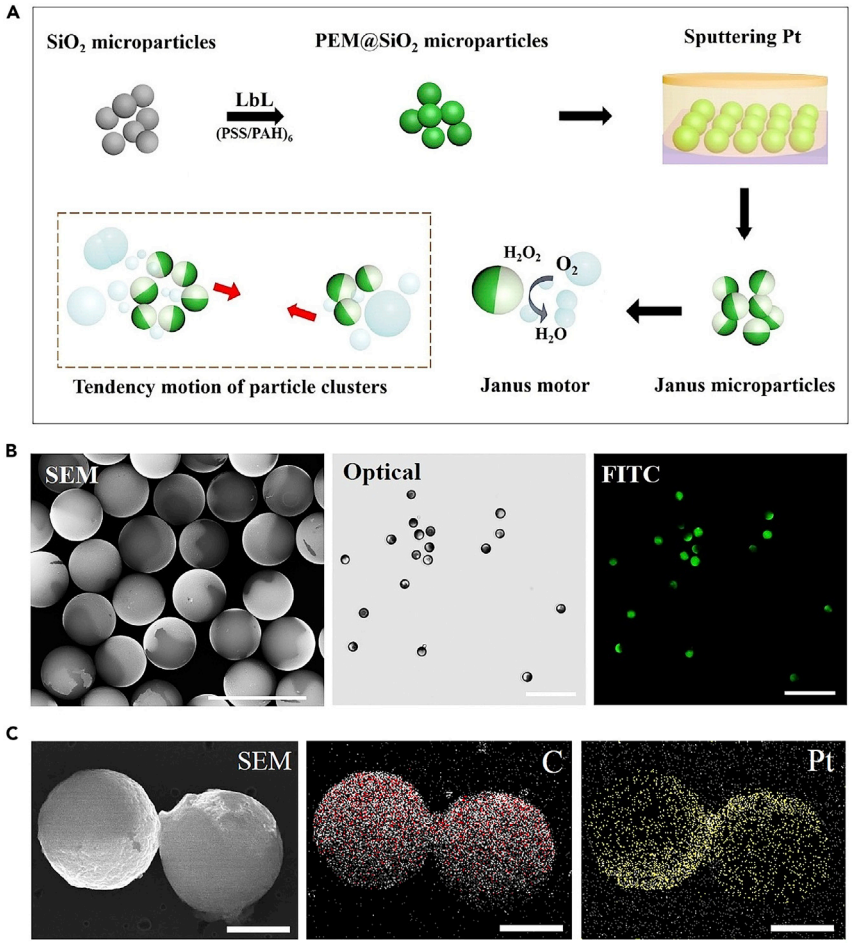

Figure 1. The experimental fabrication of Janus microparticles

(A) Schematic representation of layer-by-layer fabrication of Janus micromotors covered by Pt.

(B) SEM image, optical image, and FITC image of Janus micromotors, scale bar = 20 μm.

(C) The SEM image of the smallest cluster composed of two Janus microparticles and the EDX characterization. The scale bar is 5 μm.

half-covered by Pt. Pt catalyzes hydrogen peroxide to generate a propulsive force on the Janus micromotor and induce a strong non-equilibrium chemical gradient distribution. The self-gathering of many Janus micromotors forms a few clusters which have different activity levels. A low concentration of H_2O_2 distributed along a tubular zone that connects two nearest-neighboring clusters acts like a communication channel between them so that they are attracted to each other without external field stimuli.

RESULTS

Experimental fabrication and characterization

A polyelectrolyte multilayer Janus sphere was fabricated on monodispersed SiO_2 particles using the layer-by-layer method.[34] Alternating adsorption of positively charged poly (allylamine hydrochloride) (PAH) and negatively charged poly (styrenesulfonate) sodium salt (PSS) onto SiO_2 spheres was carried out in 2-mg mL^{-1} polyelectrolyte solution containing 0.5-M NaCl. Silica particles coated with six layers of PAH/PSS were fabricated by repeating this procedure six times. The multilayer particles were spread on a glass slide and sputtered with Pt particles on one side to fabricate the Janus particles (Figure 1A). Pt serves as an effective catalyst to speed up decomposition of hydrogen peroxide into water and oxygen gas, producing oxygen bubbles on the Pt-coated side to propel the Janus micromotor forward. The Pt loading amount was controlled with high-pressure sputtering. Scanning electron microscopy (SEM), optical imaging, and fluorescein isothiocyanate (FITC) fluorescence imaging showed the Janus colloids had an approximate radius

of 5 μm and a finely structured semi-spherical Pt shell (Figure 1B). Figure 1C shows the energy-dispersive X-ray (EDX) characterization of the smallest cluster composed of two Janus microparticles.

Synthesis and analysis of the predator-prey behavior of two clusters

We fabricated Pt-coated Janus micromotors using the layer-by-layer method[34] and dissolved them in hydrogen peroxide (H_2O_2) solution. In 15% hydrogen peroxide solution, the dispersed micromotors move randomly under the propulsion of oxygen bubbles from the beginning. Then they gradually gather to form different clusters under bubble propulsion force and diffusiophoretic force resulting from the gradient of H_2O_2 (Figure 2A). We counted the number of clusters for a given size that enclosed certain finite number of micromotors and computed its percentage in the total number of clusters. As Figure 2B shows, the big clusters that contain about 120 and 80 Janus micromotors occupie more than 19%, which is comparable with the number of clusters composed of only two micromotors. This distribution is recorded in the later stage of experiment in which many clusters have already been formed. These clusters can sense the concentration gradient of H_2O_2 induced by other clusters as far as 1000 μm away. Figure 2A records the coalescence of two clusters (a big cluster composed of about 100 micromotors enclosed by white dashed circle and a small cluster composed of about 20 micromotors enclosed by a red dashed circle) that are separated from each other over a distance about 1000 μm (see supplemental information Video S1). The small cluster is dragged by the diffusiophoretic flow toward the big cluster until they finally meet to form one giant cluster with a radius of approximately 100 μm; we call this phenomenon a predator-prey phenomena. Figure 2C recorded the decreasing distance between the two clusters, which shows a slow motion in the early stage. With respect to the time points at 1s and 1.5s in Figure 2C, the small cluster jiggles around a local point by deforming itself instead of moving forward. The minimal velocity values in Figure 2D correspond exactly to the translation stoppage of the small cluster at the moments 0.45 s, 0.95 s, and 1.5 s. In later period after 1.8s, the small cluster moves at a high speed of approximately 500 μm/s toward the big cluster without any stopping. The closer the small cluster is to the target big cluster, the faster it moves, until the measured average velocity increases up to 500 μm/s when the two clusters fuse into each other.

The predator-prey phenomena showed in Figure 2A is recorded for a high concentration of 15% H_2O_2 in the later stage of H_2O_2 solution consummation. As a comparison, the cluster formation and cluster movement in the early stage are also recorded (Figure 2E) for a low concentration of 10% H_2O_2 starting from the moment the droplet is spread on substrate (see supplemental information Video S2). Figure 2F showed the statistical distribution of cluster size. The total number of small clusters composed of less than six micromotors occupies more than 50% within the total number of clusters. Large clusters composed of 120 micromotors only occupy 3.75%, and so do the intermediate-sized clusters composed of 50, 60, or 80 micromotors. Figure 2E recorded a big cluster (moving along the blue track) chasing after a small cluster (moving along the green track), in which the outlines of both the two clusters fluctuate strongly, showing a different behavior from that of the stable clusters in Figure 2A. The distance between the two clusters decreases slowly before 5.5s, as showed in the distance-time curve in Figure 2G and the velocity-time curve in Figure 2H. The decreasing velocity of distance between the two clusters grows faster than 40 μm/s after 5.5s, which is much slower than the minimum speed of the stable clusters in high concentration of H_2O_2, as showed in Figure 2D. However, in both the high concentration and low concentration of H_2O_2, the decreasing speed of the distance between two clusters grows faster when the distance between them is shortened (Figures 2D and 2H.).

Theoretical analysis and simulation for the fusion of two clusters

The self-propulsion mechanism of active cluster is the resultant interaction of bubble propulsion force and diffusionphoresis osmotic pressure. In Figure 3A, the Pt-coated hemisphere of a Janus micromotor catalyzes H_2O_2 to generate an oxygen bubble on the Pt shell. The oscillating bubble generates a fluctuating propulsive force F_{Bubble} pointing from the Pt-coated hemisphere to the other hemisphere. The H_2O_2 concentration around the Janus micromotor distributed near the substrate, which decreases from the far region to the center of the Janus particle. This concentration gradient results in a diffusionphoresis osmotic pressure that pushes one Janus particle to another one; we called this force the diffusiophoretic osmotic force and labeled it by F_{Diffu} in Figure 3B. A single Janus micromotor undergoes stochastic transitory motion because the diffusiophoretic osmotic force F_{Diffu} is much weaker than the bubble propulsive force F_{Bubble}, which is randomly oriented. However, the two far-separated Janus micromotors tend to approach each other over a long time (Figure 3A). Once the oxygen bubbles of two nearest-neighboring Janus particles meet, the capillary attraction between the two contacting bubbles drives them to fuse into one big bubble, dragging the separated Janus particles closer to each other (Figure 3B). The self-propulsion force

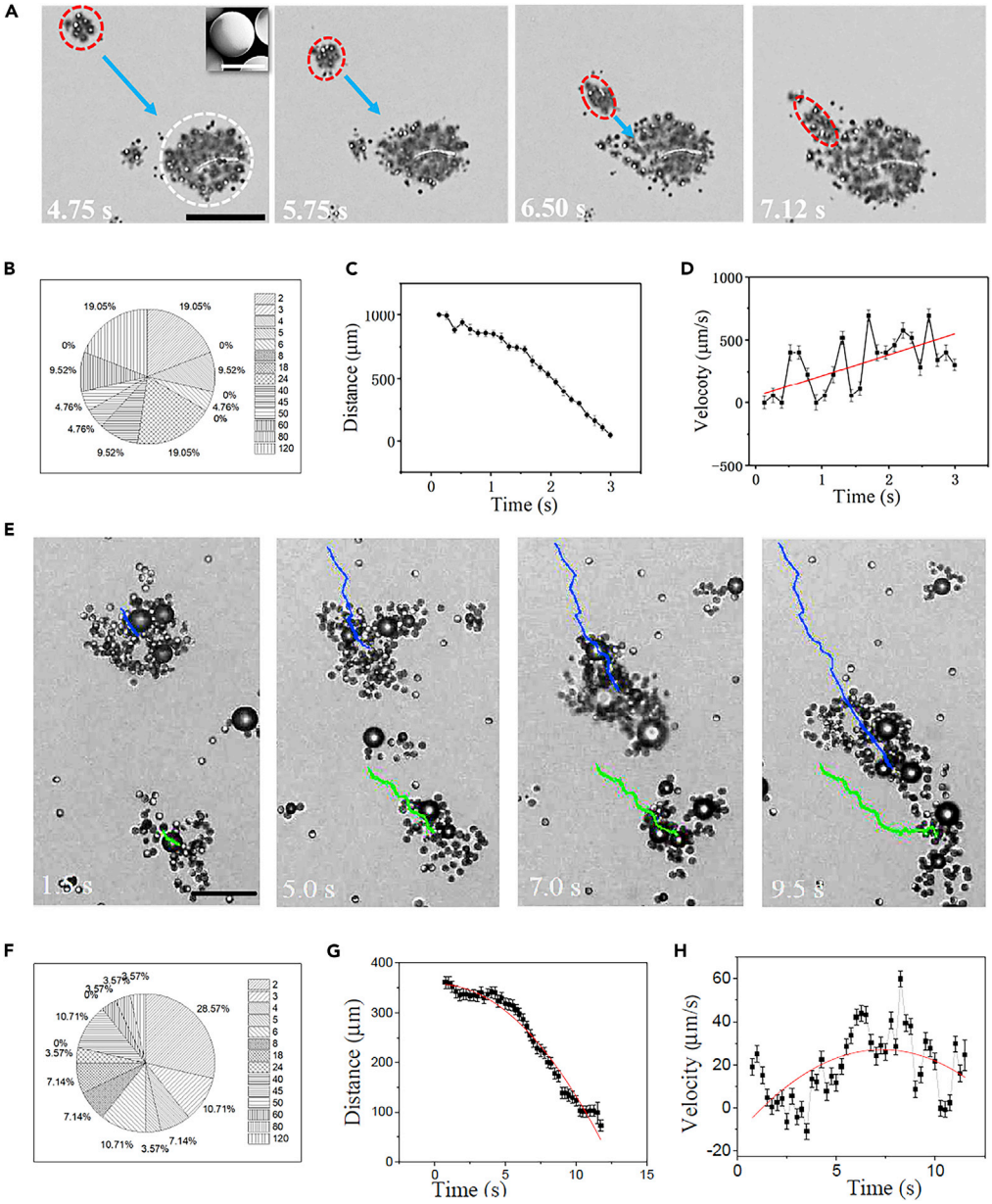

Figure 2. The predator-prey behavior of two active clusters in different H_2O_2 concentration

(A) The recorded predator-prey dynamics of self-propelled clusters in 15% H_2O_2 concentration. The scale bar represents 100 μm, and the embedded scale bar is 5 μm.

(B) The percentage of clusters with different sizes within the total number of clusters.

(C) The distance between the small cluster (enclosed by the red dashed circle in Figure 2A at 4.75s) and the big cluster (enclosed by the white dashed circle in Figure 2A at 4.75s) against time.

(D) Velocity of the small cluster (enclosed by the red dashed circle in Figure 2A at 4.75s) against time.

(E) The recorded predator-prey dynamics of self-propelled clusters in 10% H_2O_2 concentration. The scale bar is 100 μm.

(F) The percentage of the number of clusters with respect to certain size within the total number of clusters.

(G) The distance between the two clusters (one is labeled by blue track, and the other is labeled by green track) against time.

(H) The velocity of distance reduction between two clusters in Figure 2E.

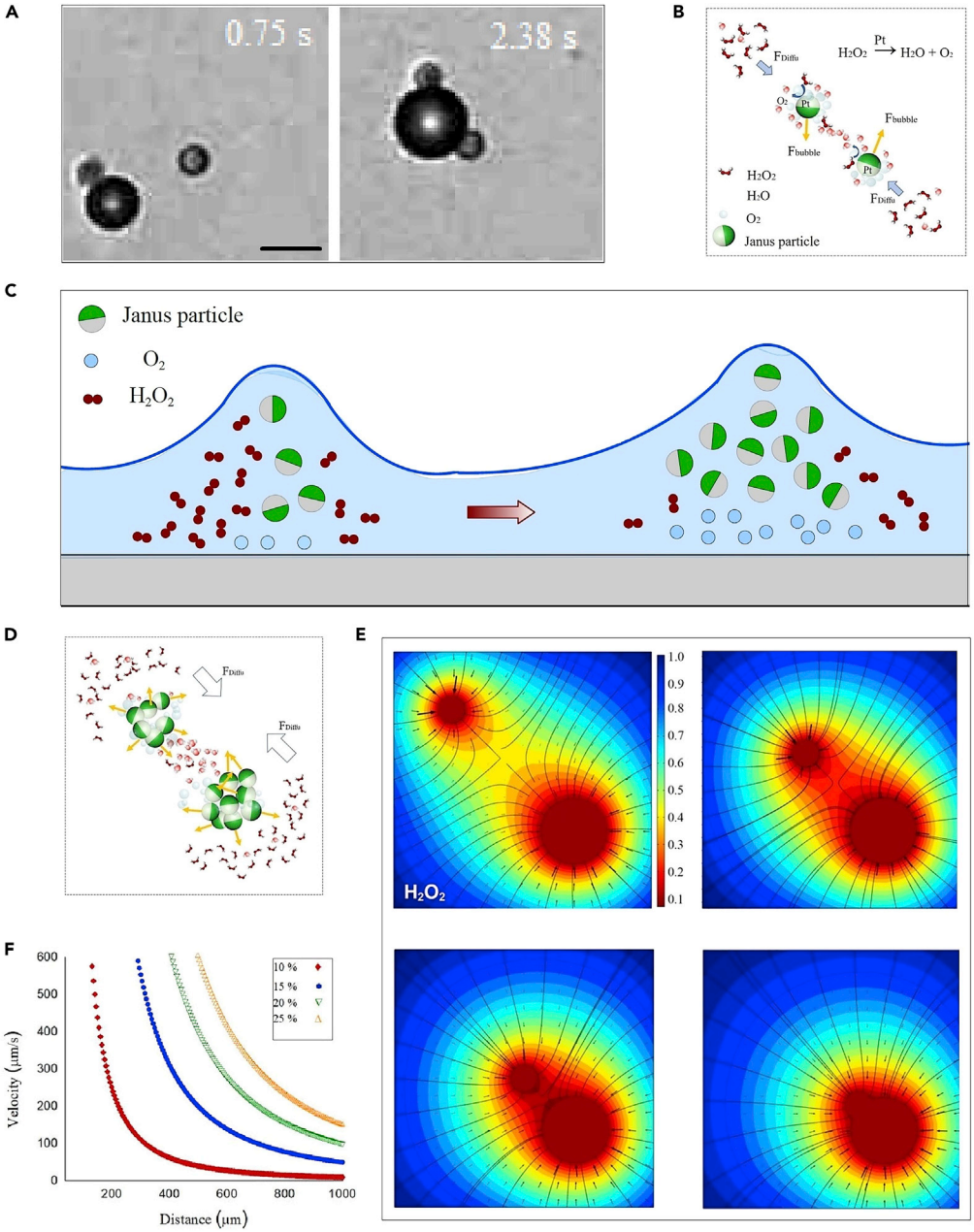

Figure 3. The theoretical analysis on the interaction mechanism between two clusters

(A) The recorded fusion of two separated micromotors under propulsion of bubble. The scale bar is 10 μm.

(B) The scheme to show the chemical gradient H_2O_2 around the two micromotors; the diffusionphoresis osmotic pressure is weaker than bubble propulsion force in the case of small clusters made of a few numbers of micromotor.

(C) The scheme to show the diffusionphoresis osmotic pressure between two Janus clusters (a small cluster on the left-hand side and a big cluster on the right-hand side) from the side view.

(D) The scheme to show the diffusionphoresis osmotic pressure and bubble propulsion forces around two clusters from top view. The bubble propulsion forces on individual Janus micromotors are randomly oriented.

(E) The numerical simulation of the concentration gradient of H_2O_2 around the two clusters with respect to different distances.

(F) The theoretical computation of the velocity of moving cluster with respect to different concentrations.

of the stable clusters (Figure 3A) in high concentration of H_2O_2 is dominated by diffusionphoresis osmotic pressure. The thin film of solution confined the cluster closer to the substrate, which results in a diffusionphoresis osmotic flow (as showed in Figure 3B, the side view of molecule distributions around the two clusters), pushing the small cluster in Figure 3C to the big cluster (Figure 3C) by the diffusionphoresis osmotic pressure (indicated by the red arrow in Figure 3C). Based on the experimental observation and data analysis of recorded videos (supplemental information, Videos S1, S2, and S3), the bubble keeps exploding to push the Janus micromotor into a random direction. We found that the bubble propulsion force vectors on individual Janus micromotor within a cluster are randomly oriented, as depicted in Figure 3D. When the bubbles fuse into one big bubble, the Janus micromotors circling around the big bubble always move in opposite direction. Therefore, these bubble propulsion force vectors cancel each other, and the resultant bubble propulsive force on the cluster finally reduced to almost zero.

The diffusiophoretic osmotic pressure dominates the cluster motion since it is independent of the collective bubble configurations. When two clusters draw closer to each other, a tubular zone with low H_2O_2 concentration forms to bridge the two clusters. The local concentration of H_2O molecules inside the tubular zone is higher than that far away from the two clusters, resulting in diffusiophoretic osmotic pressure that pushes the two clusters toward each other (see Figure 3D, the top view of molecule distributions). Figure 3E shows the numerically simulated concentration distribution of H_2O_2 that induces the diffusiophoretic osmotic pressure around the two clusters, with red indicating low concentration and blue representing high concentration of H_2O_2. The high concentration far from the region around the two clusters causes a strong chemical gradient to push the two clusters into the tubular channel, producing an effective attractive force between them. In the meantime, a higher surface tension is also generated in the tubular zone due to the dipolar attraction between water molecules, which also contributes to an important part of the attractive force between two clusters. To build an approximated theory for the velocity of the cluster, we assume that the velocity of cluster is proportional to the diffusiophoretic osmotic flow toward the big cluster. An approximated equation of H_2O_2 concentration distribution in a catalytic process is assumed as $C_{[H2O2]}(r) = C_{[H2O2]}\ (1 - b/r)$,[35] where r is the distance from a given point to the center of the cluster, b is a fitting parameter, $C_{[H2O2]}$ is the initial concentration, and $C_{[H2O2]}(r)$ is the H_2O_2 concentration distribution. The velocity of the diffusiophoretic flow is approximated using the H_2O_2 concentration gradient with the formula $V(r) = k\ b\ C_{[H2O2]}/r^2$, which is plotted in Figure 3F with respect to different initial concentration values from 10% to 25%. This theoretical approximation shows increasing velocity with decreasing distance, qualitatively agreeing with our experimental measurement. Figure 3F also shows the velocity of cluster in a high H_2O_2 concentration is much faster than that in a low H_2O_2 concentration, approximately agreeing with the measured velocity for different concentrations in Figures 2D and 2H.

The self-deformation of a moving cluster

When the small cluster (enclosed by the white outline curve Figure 4A) is pushed to the big predator cluster (the cluster in the right corner of Figure 4A), the shape of the small cluster constantly changes in response to the external flow environment (Figure 4B), acting similarly to white blood cells chasing bacteria. The aspect ratio of the outline of the small cluster fluctuates from 0.6 to 2 as measured in Figure 4C. The corresponding velocity of the small cluster increases in Figure 4D. To find out the optimal aspect ratio for the cluster to achieve maximum speed, we calculated the correlation function between aspect ratios and the corresponding velocities at the same time node according to the correlation equation,

$$Correl = \frac{\sum (a - \bar{a})(u - \bar{u})}{\sqrt{\sum (a - \bar{a})^2 (u - \bar{u})^2}},$$

where $\bar{a}$ is the average aspect ratio and $\bar{u}$ is the average velocity. Figure 4E shows that the value of the measured correlation function is always negative. This suggests that the fast-moving small cluster prefers to form a symmetrical shape instead of an anisotropic shape.

The active predator-prey behavior of a giant cluster

We also observed a giant cluster (the same giant cluster enclosed in white dashed circle in Figure 2A) actively moving around to devour other small clusters (Figure 5), mimicking exactly a predator-prey behavior (see SI Video S3). The giant cluster with an approximate radius of 100 μm is a predatory cluster capable of sensing the two tiny clusters in its neighborhood, each of them covering a tiny disc area with a radius of 14 μm. The giant cluster first moves at a speed of 14.5 μm/s to seize one tiny cluster and then

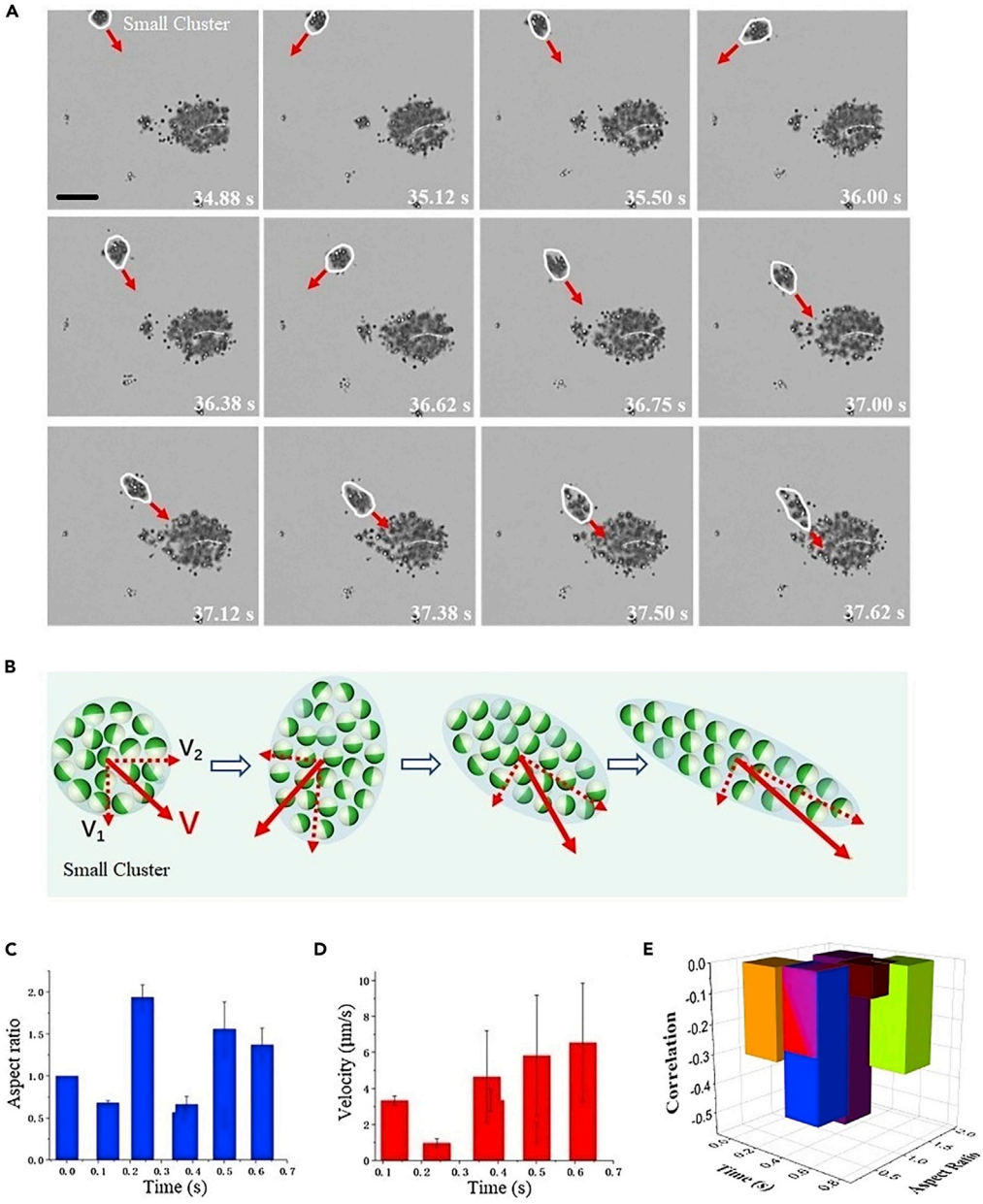

Figure 4. The self-deformation process of a moving cluster

(A) Time-lapse optical microscopic images, the outline of the moving clusters (indicated by the white enclosed circle), and its instantaneous velocity before it collides with big cluster. The scale bar is 100 μm.

(B) The scheme to show the deformation of the small cluster and its instantaneous velocity.

(C) Measured aspect ratio of the moving cluster.

(D) The velocity of the moving cluster at the same time points in (C).

(E) The correlation between aspect ratio and velocity of the moving cluster.

switches to devour the other one at a speed of 13.3 μm/s, acting like an intelligent swarming cluster. It takes 6 s for the jiggling big cluster to reach the first tiny cluster (Figure 5) and another 4 s to seize the other tiny cluster. The jiggling giant cluster shows greater mobility than the tiny clusters, which only oscillate around a local point. Based on an observation on the micromotor distribution within one cluster, we concluded that the giant cluster floats on a layer of oxygen bubbles on the substrate, acting like a steam boat on the substrate. Therefore, its mobility is much higher than the tiny cluster which generates few oxygen bubbles and failed to escape from the confinement potential near the substrate. The collective intelligent behavior of

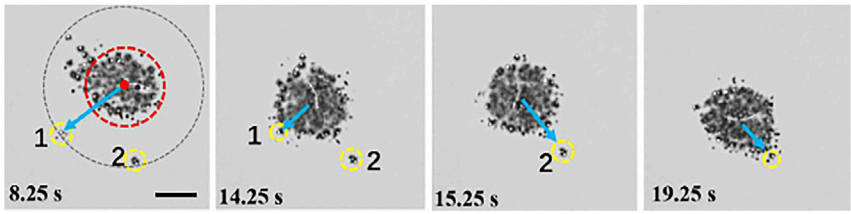

Figure 5. The active big moving cluster predates small clusters

Time-lapse optical microscopic images of the big cluster (enclosed by the red dashed circle) capturing its neighboring small clusters (enclosed by the yellow dashed circle). The scale bar is 100 μm.

the giant cluster is essentially motivated by the spatial distribution of chemical gradient in solution. The oxygen bubbles around the cluster self-gathered to form a gas layer that levitated the cluster, making the deformation of the cluster easier.

DISCUSSION

In summary, actively wandering clusters of many Janus micromotors act as predators to hunt other clusters and devour them, demonstrating a collective intelligence similar to fish schools or flocks. The fast decomposition of hydrogen peroxide in the vicinity of a cluster results in a local minimal concentration of H_2O_2, which extends to form a tubular low-concentration zone to another cluster. This low H_2O_2 concentration zone induces a diffusiophoretic osmotic pressure that pushes the two clusters far separated from each other to fuse into one. The oxygen bubbles around big clusters generate high buoyance force to counterbalance the local confinement potential near the substrate, which increases the mobility of big clusters. On the contrary, a tiny cluster composed of less than ten micromotors generates less oxygen bubbles, resulting in smaller buoyance force and less mobility. The predator-prey dynamics of swarming micromotors is not limited by materials; micromotors made of MnO_2[36,37] are also a promising candidate for collective swarming. These swarming dynamic sheds light on the physiochemical mechanism of collective intelligence in biology. The combination of this active swarming system induced by chemotaxis with the passive swarming system under external controls[38] will provide more versatile designs for massive drug delivery.

Limitations of the study

In this study, a rigorous control of fuel concentration during catalytic reaction in an open environment is of crucial importance to the behavior of self-propelled clusters. However, there are many environmental factors out of control, such as the fluctuating evaporation process of solution, the spatial fluctuation of microparticle distribution, and the fluctuating activity of enzyme. We currently only have a rough estimation for the time evolution of fuel concentration.

STAR★METHODS

Detailed methods are provided in the online version of this paper and include the following:

- KEY RESOURCES TABLE
- RESOURCE AVAILABILITY
  - Lead contact
  - Materials availability
  - Data and code availability
- EXPERIMENTAL MODEL AND SUBJECT DETAILS
- METHOD DETAILS
  - The synthesis method
- QUANTIFICATION AND STATISTICAL ANALYSIS

SUPPLEMENTAL INFORMATION

Supplemental information can be found online at https://doi.org/10.1016/j.isci.2023.106112.

ACKNOWLEDGMENTS

The authors thank the National Nature Science Foundation of China (HIT: 21603047), Natural Science Youth Foundation of Jiangsu Province (BK20191001), Heilongjiang Provincial Natural Science Foundation of China (YQ2020B001), and Jiangsu Normal University for the startup grant of He Wenping (17XLR026).

Consent for publication: All authors gave their consent for publication.

AUTHOR CONTRIBUTIONS

Z.W. Wu performed the experiment; T.Y. Si did data analysis and numerical simulations; T.Y. Si and W.P. He wrote the manuscript; Q. He conceived the project and supervised the manuscript. All authors have given approval to the final version of the manuscript.

DECLARATION OF INTERESTS

The authors declare no conflict of interest.

Received: August 2, 2022
Revised: November 9, 2022
Accepted: January 28, 2023
Published: February 3, 2023

REFERENCES

1. Bialek, W., Cavagna, A., Giardina, I., Mora, T., Silvestri, E., Viale, M., and Walczak, A.M. (2012). Statistical mechanics for natural flocks of birds. Proc. Natl. Acad. Sci. USA *109*, 4786–4791. https://doi.org/10.1073/pnas.1118633109.

2. Bazazi, S., Buhl, J., Hale, J.J., Anstey, M.L., Sword, G.A., Simpson, S.J., and Couzin, I.D. (2008). Collective motion and cannibalism in locust migratory bands. Curr. Biol. *18*, 735–739. https://doi.org/10.1016/j.cub.2008.04.035.

3. Visscher, P.K., and Camazine, S. (1999). Collective decisions and cognition in bees. Nature *397*, 400. https://doi.org/10.1038/17047.

4. Whitesides, G.M., and Grzybowski, B. (2002). Self-assembly at all scales. Science *295*, 2418–2421. https://doi.org/10.1126/science.1070821.

5. Vicsek, T., and Zafeiris, A. (2012). Collective motion. Phys. Rep. *517*, 71–140. https://doi.org/10.1016/j.physrep.2012.03.004.

6. Zhang, H.P., Be'er, A., Florin, E.L., and Swinney, H.L. (2010). Collective motion and density fluctuations in bacterial colonies. Proc. Natl. Acad. Sci. USA *107*, 13626–13630. https://doi.org/10.1073/pnas.1001651107.

7. Theers, M., Westphal, E., Qi, K., Winkler, R.G., and Gompper, G. (2018). Clustering of microswimmers: interplay of shape and hydrodynamics. Soft Matter *14*, 8590–8603. https://doi.org/10.1039/c8sm01390j.

8. Parrish, J.K., Viscido, S.V., and Grünbaum, D. (2002). Self-organized fish schools: an examination of emergent properties. Biol. Bull. *202*, 296–305. https://doi.org/10.2307/1543482.

9. Ibele, M., Mallouk, T.E., and Sen, A. (2009). Schooling behavior of light-powered autonomous micromotors in water. Angew Chem. Int. Ed. Engl. *48*, 3308–3312. https://doi.org/10.1002/anie.200804704.

10. Wang, W., Duan, W., Ahmed, S., Sen, A., and Mallouk, T.E. (2015). From one to many: dynamic assembly and collective behavior of self-propelled colloidal motors. Acc. Chem. Res. *48*, 1938–1946. https://doi.org/10.1021/acs.accounts.5b00025.

11. Mou, F., Li, X., Xie, Q., Zhang, J., Xiong, K., Xu, L., and Guan, J. (2020). Active micromotor systems built from passive particles with biomimetic predator-prey interactions. ACS Nano *14*, 406–414. https://doi.org/10.1021/acsnano.9b05996.

12. Yan, J., Chaudhary, K., Chul Bae, S., Lewis, J.A., and Granick, S. (2013). Colloidal ribbons and rings from Janus magnetic rods. Nat. Commun. *4*, 1516. https://doi.org/10.1038/ncomms2520.

13. Zhou, H., Mayorga-Martinez, C.C., Pané, S., Zhang, L., and Pumera, M. (2021). Magnetically driven micro and nanorobots. Chem. Rev. *121*, 4999–5041. https://doi.org/10.1021/acs.chemrev.0c01234.

14. Xie, H., Sun, M., Fan, X., Lin, Z., Chen, W., Wang, L., Dong, L., He, Q., Dong, L., and He, Q. (2019). Reconfigurable magnetic microrobot swarm: multimode transformation, locomotion and manipulation. Sci. Robot. *4*, eaav8006. https://doi.org/10.1126/scirobotics.aav8006.

15. Hong, Y., Diaz, M., Córdova-Figueroa, U.M., and Sen, A. (2010). Light-driven titanium-dioxide-based reversible microfireworks and micromotor/micropump systems. Adv. Funct. Mater. *20*, 1568–1576. https://doi.org/10.1002/adfm.201000063.

16. Lin, Z., Si, T., Wu, Z., Gao, C., Lin, X., and He, Q. (2017). Light-Activated active colloid ribbons. Angew. Chem., Int. Ed. *56*, 13517–13520. https://doi.org/10.1002/anie.201708155.

17. Ahmed, S., Gentekos, D.T., Fink, C.A., and Mallouk, T.E. (2014). Self-assembly of nanorod motors into geometrically regular multimers and their propulsion by ultrasound. ACS Nano *8*, 11053–11060. https://doi.org/10.1021/nn5039614.

18. Li, Z., Zhang, H., Wang, D., Gao, C., Sun, M., Wu, Z., and He, Q. (2020). Reconfigurable assembly of active liquid metal colloidal cluster. Angew Chem. Int. Ed. Engl. *59*, 19884–19888. https://doi.org/10.1002/anie.202007911.

19. Du, X., Yu, J., Jin, D., Chiu, P.W.Y., and Zhang, L. (2021). Independent pattern formation of nanorod and nanoparticle swarms under an oscillating field. ACS Nano *15*, 4429–4439. https://doi.org/10.1021/acsnano.0c08284.

20. Ma, F., Wang, S., Wu, D.T., and Wu, N. (2015). Electric-field-induced assembly and propulsion of chiral colloidal clusters. Proc. Natl. Acad. Sci. USA *112*, 6307–6312. https://doi.org/10.1073/pnas.1502141112.

21. Yan, J., Han, M., Zhang, J., Xu, C., Luijten, E., and Granick, S. (2016). Reconfiguring active particles by electrostatic imbalance. Nat. Mater. *15*, 1095–1099. https://doi.org/10.1038/nmat4696.

22. Duan, W., Liu, R., and Sen, A. (2013). Transition between collective behaviors of micromotors in response to different stimuli. J. Am. Chem. Soc. *135*, 1280–1283. https://doi.org/10.1021/ja3120357.

23. Altemose, A., Sánchez-Farrán, M.A., Duan, W., Schulz, S., Borhan, A., Crespi, V.H., and Sen, A. (2017). Chemically controlled spatiotemporal oscillations of colloidal assemblies. Angew Chem. Int. Ed. Engl. *56*,

7817–7821. https://doi.org/10.1002/anie.201703239.

24. Kagan, D., Balasubramanian, S., and Wang, J. (2011). Chemically triggered swarming of gold microparticles. Angew Chem. Int. Ed. Engl. *50*, 503–506. https://doi.org/10.1002/anie.201005078.

25. Xu, T., Soto, F., Gao, W., Dong, R., Garcia-Gradilla, V., Magaña, E., Zhang, X., and Wang, J. (2015). Reversible swarming and separation of self-propelled chemically powered nanomotors under acoustic fields. J. Am. Chem. Soc. *137*, 2163–2166. https://doi.org/10.1021/ja511012v.

26. Ahmed, D., Baasch, T., Blondel, N., Läubli, N., Dual, J., and Nelson, B.J. (2017). Neutrophil-inspired propulsion in a combined acoustic and magnetic field. Nat. Commun. *8*, 770. https://doi.org/10.1038/s41467-017-00845-5.

27. Alapan, Y., Yasa, O., Schauer, O., Giltinan, J., Tabak, A.F., Sourjik, V., and Sitti, M. (2018). Soft erythrocyte-based bacterial microswimmers for cargo delivery. Sci. Robot. *3*, eaar4423. https://doi.org/10.1126/scirobotics.aar4423.

28. Sun, M., Fan, X., Tian, C., Yang, M., Sun, L., and Xie, H. (2021). Swarming microdroplets to a dexterous micromanipulator. Adv. Funct. Mater. *31*, 2011193. https://doi.org/10.1002/adfm.202011193.

29. Wu, C., Dai, J., Li, X., Gao, L., Wang, J., Liu, J., Zheng, J., Zhan, X., Chen, J., Cheng, X., et al. (2021). Ion-exchange enabled synthetic swarm. Nat. Nanotechnol. *16*, 288–295. https://doi.org/10.1038/s41565-020-00825-9.

30. Chen, C., Mou, F., Xu, L., Wang, S., Guan, J., Feng, Z., Wang, Q., Kong, L., Li, W., Wang, J., and Zhang, Q. (2017). Light-steered isotropic semiconductor micromotors. Adv. Mater. *29*, 1603374. https://doi.org/10.1002/adma.201603374.

31. Liang, X., Mou, F., Huang, Z., Zhang, J., You, M., Xu, L., Luo, M., and Guan, J. (2020). Hierarchical microswarms with leader–follower-like structures: electrohydrodynamic self-organization and multimode collective photoresponses. Adv. Funct. Mater. *30*, 1908602. https://doi.org/10.1002/adfm.201908602.

32. Mou, F., Zhang, J., Wu, Z., Du, S., Zhang, Z., Xu, L., and Guan, J. (2019). Phototactic flocking of photochemical micromotors. iScience *19*, 415–424. https://doi.org/10.1016/j.isci.2019.07.050.

33. Buttinoni, I., Bialké, J., Kümmel, F., Löwen, H., Bechinger, C., and Speck, T. (2013). Dynamical clustering and phase separation in suspensions of self-propelled colloidal particles. Phys. Rev. Lett. *110*, 238301. https://doi.org/10.1103/PhysRevLett.110.238301.

34. Donath, E., Sukhorukov, G.B., Caruso, F., Davis, S.A., and Möhwald, H. (1998). Novel hollow polymer shells by colloid-templated assembly of polyelectrolytes. Angew Chem. Int. Ed. Engl. *37*, 2201–2205. https://doi.org/10.1002/(SICI)1521-3773(19980904)37:16<2201::AID-ANIE2201>3.0.CO;2-E.

35. Palacci, J., Sacanna, S., Steinberg, A.P., Pine, D.J., and Chaikin, P.M. (2013). Living crystals of light-activated colloidal surfers. Science *339*, 936–940. https://doi.org/10.1126/science.1230020.

36. Zhang, Y.H., Qiu, W.X., Zhang, M., Zhang, L., and Zhang, X.Z. (2018). MnO_2 motor: a prospective cancer-starving therapy promoter. ACS Appl. Mater. Interfaces *10*, 15030–15039. https://doi.org/10.1021/acsami.8b01818.

37. Wu, Y., Si, T., Gao, C., Yang, M., and He, Q. (2018). Bubble-pair propelled colloidal kayaker. J. Am. Chem. Soc. *140*, 11902–11905. https://doi.org/10.1021/jacs.8b06646.

38. Lu, X., Wei, Y., Ou, H., Zhao, C., Shi, L., and Liu, W. (2021). Universal control for micromotor swarms with a hybrid sonoelectrode. Small *17*, 2104516. https://doi.org/10.1002/smll.202104516.

STAR★METHODS

KEY RESOURCES TABLE

REAGENT or RESOURCE	SOURCE	IDENTIFIER
Chemicals, peptides, and recombinant proteins		
poly (styrenesulfonate) sodium salt (PSS, Mw = 70,000)	Sigma-Aldrich	CAS: 25,704-18-1
poly (allylamine hydrochloride) (PAH, Mw = 50,000)	Sigma-Aldrich	CAS:71,550-12-4
fluorescein isothiocyanate (FITC)	Sigma-Aldrich	CAS: 27,072-45-3
silica spheres (diameter 5 μm)	Sigma-Aldrich	CAS:44,054
sodium chloride (NaCl)	Macklin	CAS:7647-14-5
hydrofluoric acid (HF)	Macklin	CAS:7664-39-3
H_2O_2 (30% v/v)	Sigma-Aldrich	CAS No:7722-84-1; H1009
Software and algorithms		
ImageJ	ImageJ is freely available in the public domain. No license is required.	https://imagej.nih.gov/ij/
COMSOL Multiphysics 5.6	COMSOL Co., Ltd. info.cn@comsol.com.	https://www.comsol.com/release/5.6
Origin 2017	OriginLab Corporation	https://www.originlab.com/2017

RESOURCE AVAILABILITY

Lead contact

Further information and requests for resources and reagents should be directed to and will be fulfilled by the lead contact, Tieyan Si (tieyansi@hit.edu.cn).

Materials availability

All unique/stable reagents generated in this study are available from the lead contact with a completed Materials Transfer Agreement. This study did not generate additional unique reagents.

Data and code availability

- The authors declare that the data supporting the findings of this study are available within the article and the supplemental information. All other data and additional information are available from the lead contact on reasonable request.
- This article does not report original codes.

EXPERIMENTAL MODEL AND SUBJECT DETAILS

No experimental model exists for this work.

METHOD DETAILS

SEM and EDX analysis were conducted with a Hitachi S-4300 instrument at an operating voltage of 10 keV. A drop of the sample solution was dropped on a silicon wafer for the test of Janus micromotors.

Fluorescence images were obtained using a Leica TCS SP5 II confocal laser scanning microscope (CLSM). The excitation wavelength was 488 for excitation of FITC dye.

The Olympus BX53F optical microscope, coupled with a 40× objective and relative software, was used to capture videos at room temperature. The trajectories of LbL-assembled Janus micromotors were analyzed by ImageJ software.

The synthesis method

$(PSS/PAH)_6$-coated particles were first synthesized by the layer-by-layer assembly of polyelectrolyte layers on the surface of SiO_2 particles with a diameter of 5 μm. The SiO_2 particles were alternatively suspended in 2 mg/ml PSS/PAH solution containing 0.5 M NaCl for 15 min under continuous shaking, followed by three repeated centrifugation/washing steps. The $(PSS/PAH)_6$-coated silica particles were obtained by repeating the above deposition procedure. To fabricate the Janus structures, we first drop cast a 2 mL colloidal suspension of polyelectrolyte modified silica particles (diluted in ethanol with a 1:3 ratio) onto silicon substrates tilted at an angle of 9°. The monolayer is dried via slow evaporation of the solvent at 25°C allows the beads to spread into a self-assembled monolayer. The particle-coated substrates were loaded into a vacuum chamber and 5-nm Pt were deposited by electron-beam evaporation (EMITECH K575X) in a vacuum environment at a vapor incidence angle of 30º, resulting in roughly half-coated beads.

QUANTIFICATION AND STATISTICAL ANALYSIS

Using ImageJ to measure the cluster size and count the number of clusters in S1 Videos S1, S2 and S3; Using Origin 2017 to perform data processing on the position data and velocity data. Using COMSOL Multiphysics 5.6 to simulate the concentration gradient field around two clusters.